MiRGraph: A transformer-based feature learning approach to identify microRNA-target interactions by integrating heterogeneous graph network and sequence information*

Pei Liu[1], Ying Liu[1], Jiawei Luo[1(✉)], and Yue Li[2(✉)]

[1] College of Computer Science and Electronic Engineering, Hunan University, Changsha 410083, China
luojiawei@hnu.edu.cn

[2] School of Computer Science, McGill University, Montreal, QC H3A 0C6
yueli@cs.mcgill.ca

Abstract. MicroRNAs (miRNAs) play a crucial role in the regulation of gene expression by targeting specific mRNAs, and they can function as both tumor suppressors and oncogenes depending on the specific miRNA and its target genes. Detecting miRNA-target interactions (MTIs) is critical for unraveling the complex mechanisms of gene regulation, the potential therapeutic targets and diagnostic markers. There are currently few studies on MTIs prediction that simultaneously perform feature learning on heterogeneous graph network and sequence information. Thus, we present a transformer-based multi-view feature learning method, named MiRGraph, capable of modeling both heterogeneous network and sequence features to improve the prediction performance of MTIs. To alleviate the problem of partial missing sequence information when using k-mer encoding or candidate target sites (CTSs), we utilize the mature miRNA sequence and the complete 3'UTR sequence of the target mRNAs to encode seqeunce features. And a transformer-based CNN (TransCNN) module is designed for miRNAs and genes respectively to extract their personalized sequence features. Then a heterogeneous graph transformer (HGT) module is adopted to learn the network features through extracting the relational and structural information in a heterogeneous graph consisting of miRNA-miRNA, gene-gene and miRNA-target interactions. Finally, we utilize a multilayer perceptron (MLP) to map the learned features of miRNAs and genes into a same space, and a bilinear function to calculate the prediction scores of MTIs. Comparisons with other existing MTIs prediction methods illustrate the superiority of MiRGraph under multiple standard criteria metrics. The comparing results of distinguishing the high functional MTIs and case studies on identifying the novel MTIs showcase the real-world applications of MiRGraph in biological research.

Availability:
MiRGraph is implemented in python and available at https://github.com/Liangyushi/MiRGraph.

Keywords: MiRNA-Target Interaction · Heterogeneous Graph Transformer · Deep learning · Transformer · CNN.

* Supported by the National Natural Science Foundation of China under Grant 62032007, 62372165 and 62202152.

1 Introduction

MicroRNAs (miRNAs) are endogenous, non-coding, single-stranded small RNA molecules composed of approximately 22 nucleotides, which widely participate in all kinds of biological processes such as immune response, transcription, proliferation and differentiation in human cells [1; 2; 3]. MiRNAs mainly play a key regulator at the post-transcriptional regulation by binding to the 3' UTRs of their target mRNAs, thereby inducing mRNAs degradation or inhibiting mRNA translation [4]. Their dysregulation can affect many biological characteristics in cells ultimately leading to various diseases, even cancers [5; 6]. Therefore, exploring the accurate and comprehensive miRNA-target gene interactions is of great significance for revealing the regulatory mechanism of miRNA and its dysfunction in complex diseases.

Some traditional biological methods including quantitative real-time PCR (qPCR) and microarray experiments can accurately capture the functional interactions between miRNAs and target mRNAs, while these methods are costly and time-consuming [7; 8; 9]. Furthermore, with the continuously increasing number of newly discovered miRNAs, confirming all possible miRNA-target interactions (MTIs) through such experiments is not feasible. Thus, a series of computational prediction methods were developed to detect MTIs to narrow down the candidate MTIs for experimental validation.

The computational algorithms of MTI predictions can be divided into two categories: feature extraction-based methods and deep learning-based methods. The former utilize hand-crafted features. For instance, PITA [10] leveraged site accessibility to calculate thermodynamic stability-based scores. mirSVR [11] trained a support vector regression model based on various features including sequence information, thermodynamic stability and structural accessibility. miRanda [12] utilized the sequence complementarity to assess the likelihood of MTI. TargetScan [13] prioritized the miRNA-candidate target site (CTS) using seed region matching rule. Although these feature extraction-based methods did provide candidate targets, they depended on the design of hand-crafted feature engineering strategies, resulting in inconsistent predictions and high false positive rates.

Many deep learning-based methods also used manually extracted features as input. For instance, DeepTarget [14] adopted four types of seed sequence matching rules to select CTSs, and then utilized autoencoders and stacked RNNs to learn features. The miRAW [15] applied multi-layer perceptron (MLP) to learn features using additional information like binding site accessibility energies. TargetNet [16] designed a Resnet-based deep learning framework with a novel miRNA–CTS sequence encoding scheme incorporating extended seed region alignments. Although these methods utilized CTS to reduce the search space, they rely only on the RNA sequence information and are unable to utilize the miRNA-regulatory network information. Meanwhile, with the accumulation of the relevant miRNA-mRNA interaction databases such as mirRTarBase [17; 18], TargetSan [19], StarBase [20], it has become possible to use graph neural networks to extract relational information between the two RNA species. MRMTI [21] utilized the multi-relation graph convolutional module and the Bi-LSTM module to incorporate both network topology and sequential information. SRG-Vote [22] leveraged Doc2Vec and Graph Convolutional Network (GCN) to separately generate sequential and geometrical embeddings from molecular sequences and relational network. While both methods explored network and sequence information, their k-mer based sequence representation may not be adequate. In addition to the above shortcomings, there is currently a lack of MTI prediction methods for extracting node features in heterogeneous networks by modeling structural and relational data. Moreover, while considering edge and node information simultaneously in heterogeneous graph networks has proven to be beneficial for the improvement of model performance [23; 24; 25], their applications on MTI prediction remains unexplored.

In this study, we present a novel transformer-based deep learning framework named MiRGraph, which considers both network and sequential information for MTIs prediction. Instead of relying on k-mer coding or CTSs, our method utilizes the raw sequences of mature miRNA and the 3'UTRs of target mRNAs to initialize the sequence features. To address the different sequence lengths of miRNAs and mRNAs, we design a transformer-based CNN (TransCNN) module for miRNA and mRNA respectively to extract sequence features from long sequences. Furthermore, to fully utilize the existing biological relationship data, we construct a heterogeneous graph network consisting of miRNA-miRNA, gene-gene and miRNA-target interactions. To better learn the relational and structural information in heterogeneous network, we utilize a heterogeneous graph transformer (HGT) module to capture the topological features. After concatenating these two types features of miRNAs and genes, we adopt an MLP layer to map miRNA and genes into the same embedding space and use a bilinear function to calculate the MTI prediction scores. Finally, to

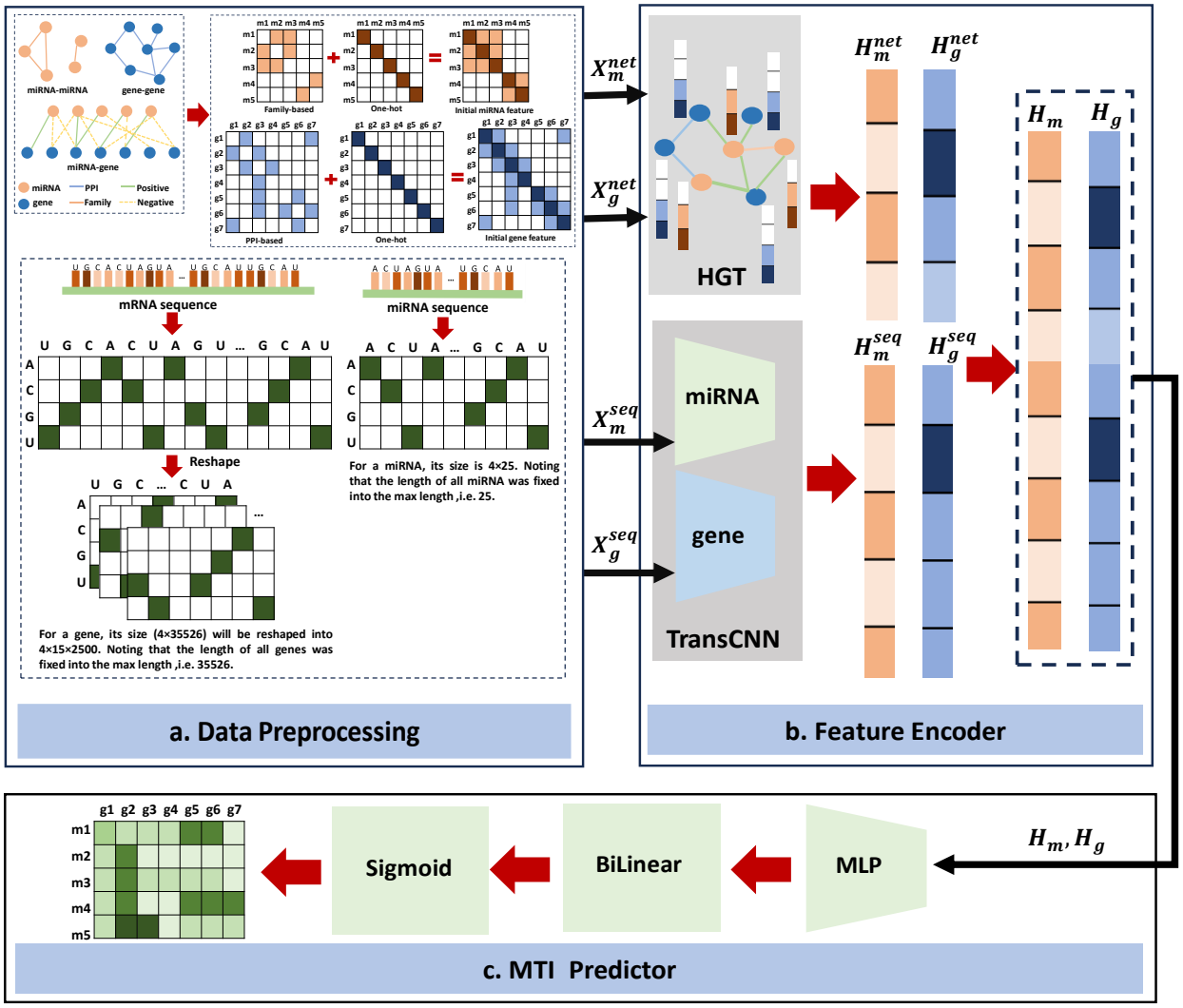

Fig. 1. Overall framework of MiRGraph.

alleviate the imbalance between positive and negative samples, we use the focal loss function [26] to train the model. The proposed method MiRGraph is compared with several existing MTIs prediction methods on two different datasets under standard metrics. The results demonstrate that our approach outperforms most of the state-of-the-art methods in MTIs prediction task. We conduct qualitative analysis to demonstrate the capability of MiRGraph in distinguishing the high functional MTIs and identifying novel MITs.

2 Method

The proposed framework MiRGraph mainly consists of three parts (Fig. 1): a. data preprocessing; b. feature encoder; and c. MTI predictor. Firstly, we use data preprocessing module to build a heterogeneous information network (HIN), and obtain the initial network and sequential embeddings of miRNAs and genes. Then, the initial embeddings are fed into feature encoder including two modules (i.e. HGT and TransCNN) to learn network and sequential representations separately. After concatenating these two types of representations, we feed them into the MLP predictor to obtain the MTIs predicting scores.

2.1 Data Preprocessing

HIN Construction. The predicted miRNA-gene interactions network is obtained from TargetScan [13; 19]. We use the experimentally validated MTI from miRTarbase [17] to label the TargetScan predicted edges as positive edges and the rest as negative edges. This results in 22,221 positive edges and 59,897 negative edges between 279 miRNAs and 14676 genes. Considering that the negative edges of the network built on this basis are too large, we retain only the negative edges for each gene g, which involves the top 10 miRNAs with sequence most similar to the miRNA involved in the positive MTI. This reduces the negative samples and improves the specificity of our model to discriminate similar but false MTI. We obtain protein-protein interaction network with 1,043,837 edges between 11,091 genes from the STRING database [27]. A miRNA-miRNA interaction network with 209 edges between 279 miRNAs is built with miRNA family information [28]. Finally, a new HIN is constructed by integrating these three networks.

Feature Initialization. We convert the miRNA sequences into one-hot representations with the maximum length set to $k_m = 25$. We process the target gene sequence in the same way with the maximum length set to $k_g = 35,526$. Because the maximum length of the complete 3'UTR sequence of all genes is too long, each gene sequence is divided into 15 fixed-length shorter sequences. As a result, for all miRNAs and genes, we obtain their initial sequence features $X_m^{seq} \in R^{279\times4\times25}$ and $X_g^{seq} \in R^{14676\times4\times15\times2500}$. This is equivalent to dividing a long 2D image into 15 segments each of height of 4 and width of 2500.

To obtain the initial miRNA-miRNA and gene-gene networks $X_m^{net} \in R^{279\times279}$ and $X_g^{net} \in R^{14676\times14676}$, we first construct the diagonal matrix based on miRNAs and genes identifiers using one-hot encoding, and then integrate them with the corresponding interaction matrix via element-wise addition (Fig. 1a).

2.2 Feature Encoder

Sequence Feature Encoding Module. For the input of gene $x_g^{seq} \in R^{14676\times4\times15\times2500}$, we have three sequential layers for the $TransCNN_gene$ (Fig. 2a):

1. First, we use two layers of 2D convolution layer $conv2d(.)$ to integrate the 15 sequence segments of each gene. This is followed by a max-pooling layer $maxpool2d(.)$ to reduce the sequence length. To effectively learn feature from the 15 sub-sequences, we introduce a channel attention mechanism layer (ECA-Net) [29] between the two $conv2d(.)$ layers. ECA-Net computes local cross-channel interaction using 1D convolution.
2. Then, we use residual connection after the 1D convolution layer $conv1d(.)$. A max-pooling layer $maxpool1d(.)$ is applied after each residual connection to further reduce the sequence length.
3. Finally, the transformer encoding layer $transformer_encoder(.)$ is adopted to learn global contextual information from the sequence feature map.

For the input of miRNAs $X_m^{seq} \in R^{279\times4\times25}$, we utilize similar operations in steps 2 and 3 in $TransCNN_gene$ to learn sequence features of miRNAs (Fig. 2b). In order to integrate the two types of sequence information, we reshape the final sequence feature embedding of miRNAs and genes to have the same embedding dimensions, i.e. $H_m^{seq} \in R^{279\times3200}$ and $H_g^{seq} \in R^{14676\times3200}$.

Network Feature Encoding Module. To better model the heterogeneity in HIN, we leverage Heterogeneous Graph Transformer (HGT) [24], which characterizes the heterogeneous attention on each edge by dedicating parameters specific to the node and edge types, giving rise to specialized representations of nodes and edges. Given the network features of miRNAs and genes $X_m^{net} \in R^{279\times279}$ and $X_g^{net} \in R^{14676\times14676}$, a linear layer $Linear(.)$ is first used to map the initial features of different types of nodes to the same space. And then they are fed into the $HGTConv(.)$ layer to obtain more fine-grained features of different types of nodes by performing the multi-headed heterogeneous attention mechanism. After two layers of $HGTConv(.)$, we obtain the final network features of miRNAs and genes, i.e. $H_m^{net} \in R^{279\times128}$ and $H_g^{net} \in R^{14676\times128}$ (see Fig. 2c).

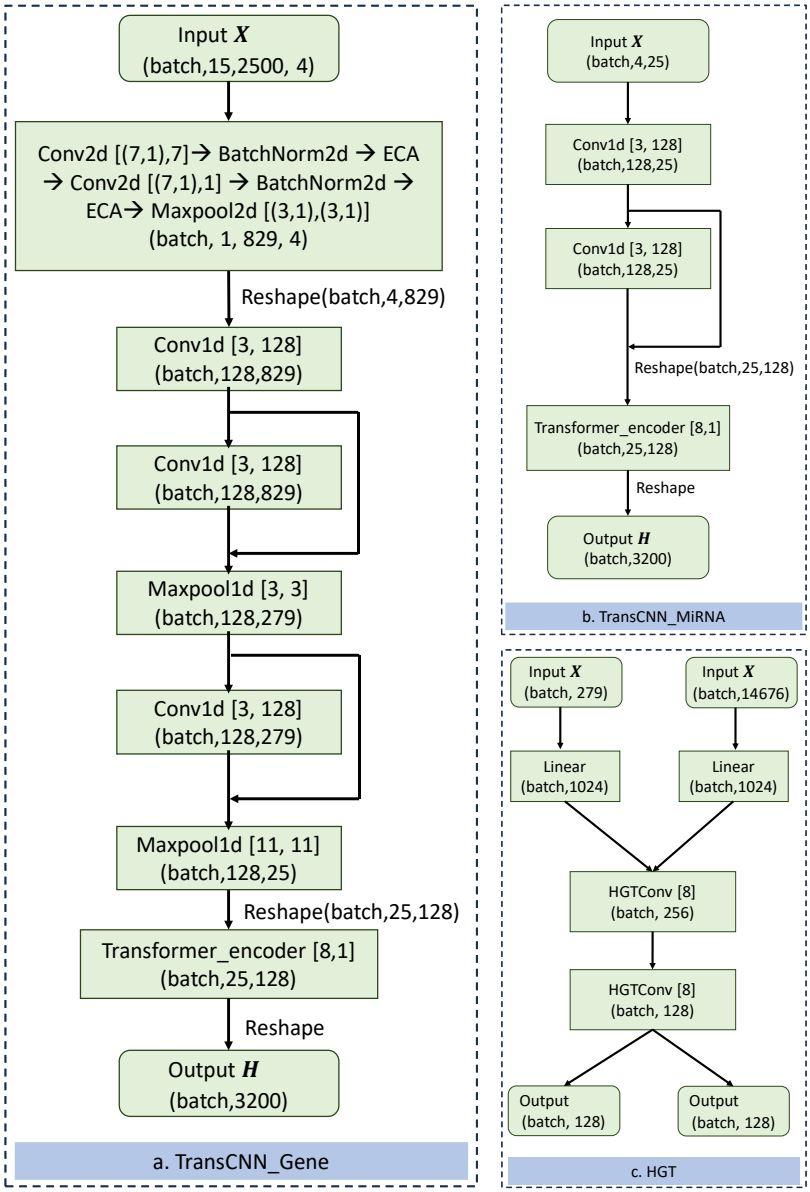

Fig. 2. Details of TransCNN and HGT in Feature Encoder.

Feature Integration Module. We first concatenate the two types of node embeddings, and then apply the nonlinear activation function $GELU(.)$ to them. We obtain the final representation of miRNAs and genes, i.e. $H_m \in R^{279\times3328}$ and $H_g \in R^{14676\times3328}$ (Fig. 1b):

$$H_m = GELU(Concat([H_m^{seq}, H_m^{net}])), \quad H_g = GELU(Concat([H_g^{seq}, H_g^{net}])) \tag{1}$$

2.3 MTI Predictor

Predicting Score. Given the input of H_m and H_g, we first use $MLP(.)$ to separately map them onto the same low-dimensional space, and then use a bilinear layer followed by sigmoid function $g(.)$ to compute the MTI probability:

$$p_{m,g} = g(MLP(H_m)^T \times W \times MLP(H_g)) \tag{2}$$

Loss Function. To account for the imbalance of small number of positive and large number of negative examples (i.e., true and false MTI edges), we use the focal loss function [26] to train the model:

$$FL(p) = \begin{cases} -\alpha(1-p)^{\gamma} log(p), & y = 1 \\ -(1-\alpha)p^{\gamma} log(1-p), & y = 0 \end{cases} \tag{3}$$

where y is the true label, p is the predicting score, $\alpha > 0$ is a hyperparameter to balance the importance of positive/negative examples, and $\gamma > 0$ is a hyperparameter. By default, we set $\alpha = 0.65$ and $\gamma = 2$.

3 Experiments

3.1 Experimental setup.

Datasets. We evaluated the proposed method with two types of experimentally verified miRNA–target interaction datasets as follows:

- **Test miRTarBase MTI**. We split the positive (miRTarbase+TargetScan) and negative edges (TargetScan only) (Section 2.1) into 70%, 20%, and 10% for training, validation and testing, respectively.
- **miRAW test MTI.** We used the processed miRAW dataset by TargetNet authors [16]. This dataset was originally derived from DIANA-TarBase [30] and miRTarBase [17]. The training set contains 26803 positive and 27341 negative pairs, a validation set contains 2385 positive and 2264 negative miRNA–CTS pairs, and each of the 10 testing sets contains 548 positive and 548 negative pairs.
- The TargetNet data also contains validated MTI based on the log-fold-change (LFC) of miRNA interference (miRNAi) experiments followed by gene expression profiling by 11 microarray and 2 RNA-seq experiments. These dataset involve distinct miRNAs from the above data, thereby providing additional validation data on our method.

Implementation details. The implementation of MiRGraph was done in Python (v 3.9.6) using Pytorch (v 1.10.0) and PyTorch Geometric (v 2.1.0) as backend. To more completely consider the heterogeneous graph structural information in the 'Test miRTarBase MTI' dataset, we did not adopt any graph sampling method including *HGTSampling* to reduce the graph size. This inevitably leads to excessive memory requirements during training, so it is not feasible to use GPU to train the entire MiRGraph. To speed up model training, we designed two training strategies as follows:

- **End-to-end training strategy.** We first pre-trained TransCNN and HGT, and then transferred the parameters of the trained HGT and TransCNN to MiRGraph for an end-to-end fine-tuning.
- **Step-by-step training strategy.** We first trained TransCNN and HGT separately, and then directly used the HGT and TransCNN to obtain network and sequence feature embeddings of miRNAs and genes. Finally, we only trained the prediction layer based on the learned feature representations to obtain the scores.

We observed that the second strategy (an average of 25 second per epoch) takes much less time than the first one (an average of 3m per epoch) while conferring similar performances. Therefore, we only demonstrated the results of the second strategy. Specifically, we first trained the HGT (taking an average of 45s per epoch) on the CPU and the TransCNN on the GPU (taking an average of 42s per epoch), and finally trained MiRGraph or the prediction layer of MiRGraph on the CPU. We used NVIDIA A100-SXM4-40GB for the GPU job, AMD EPYC 7413 24-Core for the CPU job with the memory of 256G. The experiments were performed on the Compute Canada Narval server. We leveraged Kaiming [31] as the initialization method for model parameters, AdamW as the optimizer for model training. The learning rates of HGT, TransCNN and MiRGraph were set as 0.001, 0.0001 and 0.0001 respectively.

3.2 Comparing results of different tasks

In order to comprehensively evaluate the performance of our method, we conducted two comparative experiments on two different datasets respectively, namely predicting MTIs and distinguishing high functional MTIs.

Predicting MTIs on the Test miRTarBase MTI. We compared the MTIs prediction performance on the test miRTarBase MTI using RCGN [23], MRMTI [21], HGT [24], HGT_BiSTM, TransCNN and MiRGraph. MiRGraph obtained the best prediction performance with the highest area under the ROC (AUROC) and area under the precision-recall (AUPRC) (Fig. 3). Not only MiRGraph conferred AUROC and AUPRC that are 3.38 and 4.38 percent higher than those from the runner-up method MRMTI, but also MiRGraph achieved the best performance on most other metrics (Table 1). We also observed a large overlap between the three methods of HGT, TranCNN and MiRGraph in terms of the predicted MTIs, especially in true positive MTIs and true negative MTIs (Fig. 4). Nonetheless, we observed that the number of false positive MTIs predicted by MiRGraph was much smaller than that of HGT and TranCNN (Fig. 4d). The improved specificity of MiRGraph is likely attributed to our fusion heterogeneous network and sequence features.

In addition, the performance of RGCN is significantly worse than HGT, which demonstrates the advantage of the transformer layer in learning the attention weights between different relationships to better capture the heterogeneous information in the graph network. Interestingly, comparing HGT, RGCN, HGT_BiLSTM and MRMTI, we found that the prediction performance of MRMTI (fusing graph and sequence information with RGCN and BiLSTM) is better than RGCN. On the other hand, HGT_BiLSTM (using HGT and BiLSTM to learn graph and sequence information) is worse than HGT. From the above observations, we argue that it is necessary to simultaneously extract useful graph features and the high-quality sequence features when fusing graph information and sequence information, rather than considering them separately as in HGT_BiLSTM.

Distinguishing high functional MTIs on miRAW dataset. The miRAW dataset does not have corresponding graph structure data. The gene sequence of train-validation dataset only has the experimentally

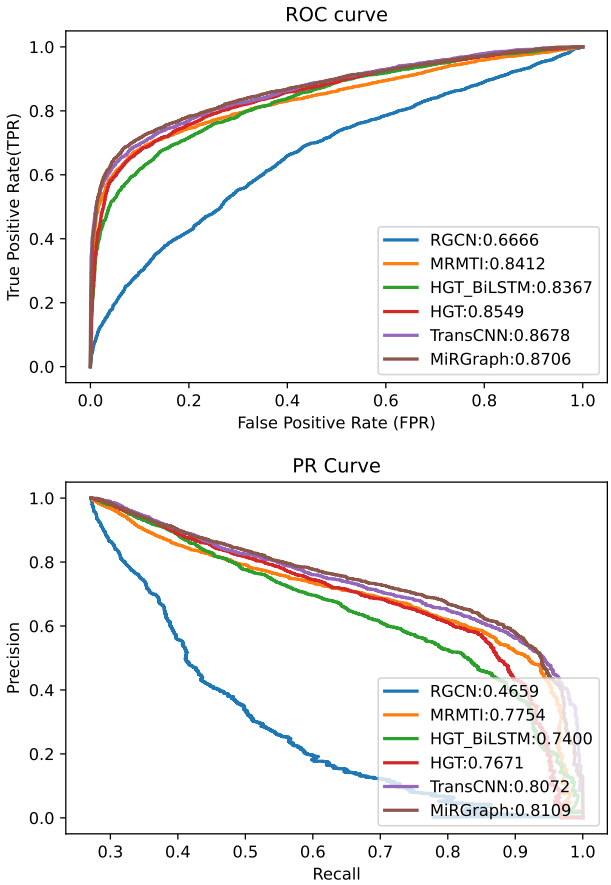

Fig. 3. The ROC and PR curves of MTI predictions on the test miRTarBase MTI data.

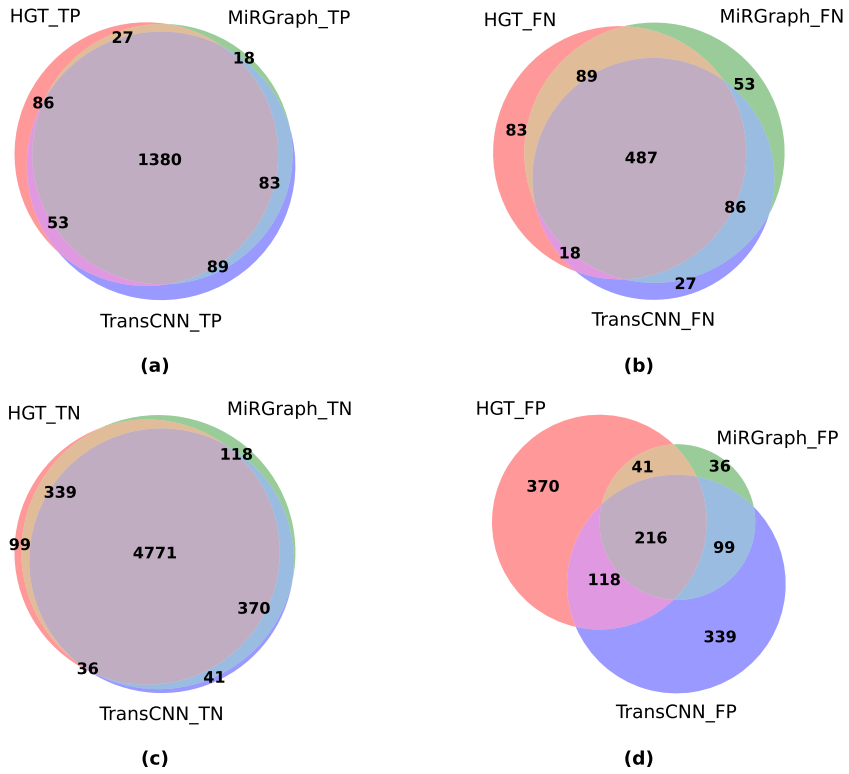

Fig. 4. Venn diagram comparing HGT, TranCNN and MiRGraph predicted MTI. TP, TN, FP and FN stand for True positive, True Negative, False Positive, and False Negative, respectively. HGT_TP, MiRGraph_TP and TransCNN_TP indicate the number of TP predicted by HGT, MiRGraph and TransCNN respectively. Panel a-d display the 3-way overlap of TP, FN, TN, and FP among HGT, MiRGraph, and TransCNN, respectively.

Table 1. Comparison of MTIs perdiction performance on the new MTIs dataset.

	Precision	Recall	F1	Accuracy	FPR	Specificity	Negative Precision
RGCN	0.4686	0.3900	0.4257	0.7152	0.1641	0.8359	0.7869
MRMTI	0.7337	0.6716	0.7013	0.8451	0.0905	0.9095	0.8818
HGT_BiLSTM	0.6425	0.6631	0.6526	0.8090	0.1369	0.8631	0.8735
HGT	0.6748	0.6955	0.6850	0.8269	0.1244	0.8756	0.8857
TransCNN (ours)	0.6752	**0.7220**	0.6978	0.8308	0.1289	0.8711	**0.8941**
MiRGraph (ours)	**0.7937**	0.6784	**0.7315**	**0.8652**	**0.0654**	**0.9346**	0.8867

verified CTSs. Therefore, we chose to evaluate the performance of only TransCNN_miRNA (a module in MiRGraph; Fig. 2b) in distinguishing high functional MTIs on this dataset. We first trained model on the miRAW train-validation dataset, and then based on the independent LFC test dataset, we compared the ability of TargetNet [16] and TransCNN_miRNA on distinguishing high functional MTIs through examining the correlation between the level of expression down-regulation and the top-ranked prediction scores. We first ranked each miRNA-mRNA pair in the LFC dataset based on the MTIs prediction scores, and examined the average of the LFC values of their expression among the top ranked predicted MTIs (Fig. 5). The top predicted target genes from TargetNet and TransCNN_miRNA exhibit negative LFC, indicating down-regulation of the candidate target genes by the transfected miRNAs. Compared to TargetNet, the top target genes identified by TransCNN_miRNA exhibit more negative LFC, implying that they are more likely to be the true targets of the miRNAs.

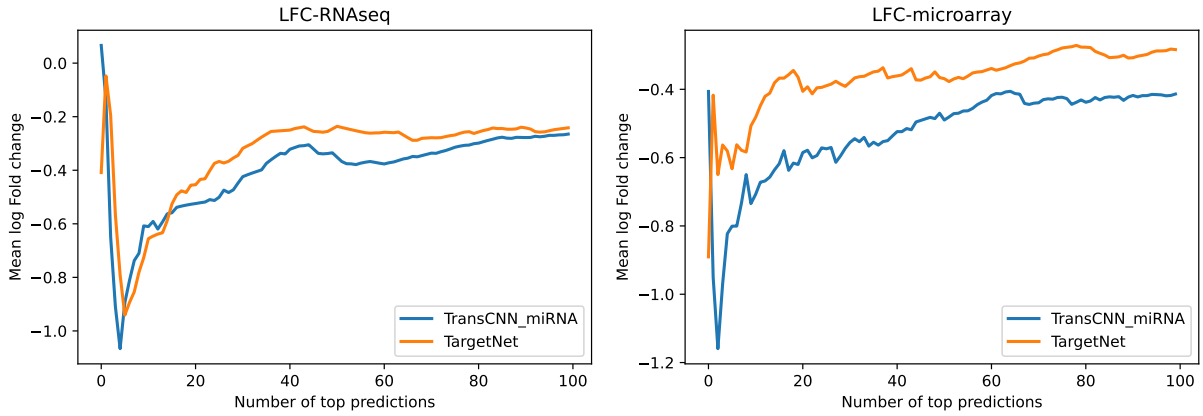

Fig. 5. LFC of top 100 target genes predicted by TransCNN_miRNA and TargetNet. The lower the LFC the more down-regulated the target genes are due to the miRNA transfection in HeLa or HEK329 cells and therefore the more likely the target genes being the true miRNA targets.

Table 2. Top five candidate genes/miRNAs predicted by MiRGraph for *hsa-miR-335-5p* and *BRCA1*.

miRNA	gene	evidence
hsa-miR-122-5p	SOCS1	PMID: 23348614
	PPP1R11	–
	PDIA6	–
	ANKRA2	–
	DEFB108B	–
hsa-miR-302d-3p	BRCA1	–
hsa-miR-302a-3p		–
hsa-miR-373-3p		–
hsa-miR-181a-5p		PMID: 23622248
hsa-miR-520a-3p		–

3.3 Case Studies

To further demonstrate the real-world application of MiRGraph, we performed case studies namely the identification of novel MTIs. We first chose to investigate *hsa-miR-122-5p*, which is associated with cancer development and metastasis by targeting specific oncogenes [32]. Table 2 lists the top five MiRGraph-predicted target genes. Among them, *SOCS1* is supported by the existing literature as it is modulated by *hsa-miR-122-5p* in regulation of Type I interferon expression in the hepatitis C virus (HCV)-infected patients [33]. The other four novel candidate genes deserve further investigation.

Then we investigated the prediction of a specific oncogene *BRCA1*, which is a well-known hereditary gene associated with the risk of breast and ovarian cancers. Table 2 shows the top five predicted miRNAs and their supports. Interaction between *BRCA1* and *hsa-miR-181a-5p* has been found from a high-confidence high-throughput experimental assay called CLASH [34]. To further analyze the principle mechanism of MTIs prediction, we used TAM [35] to conduct functional analysis of the top-10 candidate miRNAs of *BRCA1*. We found that most of the top-10 miRNAs are under the 'Cluster', 'Family', 'Function' and 'HMDD' categories, which illustrates that these miRNAs have the same functional mechanism (Table 3). Notably, the predicted *BRCA1* miRNA regulator *hsa-miR-181a-5p* is associated with development and diseases, including 'Human embryonic stem cell (hESC) regulation', 'Glioma', 'Heart Failure' and 'Neoplasms'.

4 Discussion

The investigation on the miRNA-target interactions can help reveal the complex gene regulation and disease treatment, and so far, there are few studies that simultaneously consider multi-relationship network information and site-binding sequence information in the task of identifying functional miRNA-target interactions

Table 3. Functional analysis results of potential biological significance of top-10 candidate miRNAs of *BRCA1* using TAM version 2.0. Noting that the top-10 candidates includes *hsa-miR-302d-3p, hsa-miR-302a-3p, hsa-miR-373-3p, hsa-miR-181a-5p, hsa-miR-520a-3p, hsa-miR-302e,hsa-miR-372-3p, hsa-miR-302b-3p, hsa-miR-19b-3p and hsa-miR-520c-3p.*

Category	Term	Count	P-value	Bonferroni	FDR	miRNAs
Cluster	hsa-mir-1283 cluster	4	3.91E-03	3.13E-01	1.32E-01	hsa-mir-520a, hsa-mir-520c, hsa-mir-372, hsa-mir-373
Cluster	hsa-mir-302a cluster	3	4.48E-05	3.59E-03	4.04E-03	hsa-mir-302d, hsa-mir-302b, hsa-mir-3023
Family	mir-302 family	4	8.80E-07	7.01E-05	4.74E-04	hsa-mir-302e, hsa-mir-302d, hsa-mir-302b, hsa-mir-3023
Function	cell fate determination	4	7.28E-04	5.83E-02	3.03E-02	hsa-mir-302e, hsa-mir-302d, hsa-mir-302b, hsa-mir-302a
Function	onco-miRNAs	3	1.56E-02	1.00E+00	4.43E-01	hsa-mir-373, hsa-mir-372, hsa-mir-19b
Function	Human embryonic stem cell (hESC) regulation	6	1.58E-03	1.26E-01	6.11E-02	**hsa-mir-181a**, hsa-mir-302d, hsa-mir-302b, hsa-mir-302a, hsa-mir-373,hsa-mir-372
HMDD	Azoospermia	4	3.92E-05	3.14E-03	4.24E-03	hsa-mir-373, hsa-mir-372, hsa-mir-302a, hsa-mir-19b
HMDD	Breast Neoplasms	5	3.24E-02	1.00E+00	7.97E-01	hsa-mir-520a, hsa-mir-302d, hsa-mir-302b, hsa-mire302a, hsa-mir-19b
HMDD	Carcinoma	6	2.57E-05	2.05E-03	4.62E-03	hsa-mir-302e, hsa-mir-302d, hsa-mir-302b, hsa-mir-302a, hsa-mir-373, hsa-mir-372
HMDD	Glioma	5	3.02E-05	2.41E-03	4.08E-03	hsa-mir-373, hsa-mir-302d, **hsa-mir-181a**, hsa-mir-302a, hsa-mir-302b
HMDD	Heart Failure	8	4.73E-05	3.79E-03	3.66E-03	hsa-mir-520a, hsa-mir-520c, **hsa-mir-181a**, hsa-mir302b, hsa-mir-302a,hsa-mir-19b, hsa-mir-373, hsa-mir-372
HMDD	Neoplasms	7	2.59E-04	2.07E-02	1.56E-02	**hsa-mir-181a**, hsa-mir-302d, hsa-mir-302b, hsa-mir-302a, hsa-mir-19b,hsa-mir-373, hsa-mir-372
HMDD	Pre-Eclampsia	4	9.72E-05	7.77E-03	6.57E-03	hsa-mir-302e, hsa-mir-302d, hsa-mir-302b, hsa-mir-302a
HMDD	Skin Neoplasms	3	1.81E-05	1.45E-03	4.90E-03	hsa-mir-302d, hsa-mir-302b, hsa-mir-302a

(MTIs). We propose a multi-view deep learning approach named MiRGraph, for the prediction of MTIs. Taking into account different representation structures of sequence features, we combine transformer with Resnet architecture to design TransCNN_miRNA and TransCNN_gene feature encoding module for the specialized learning of miRNAs and genes sequence features respectively. This design is similar to Enformer [36]. However, Enformrer was designed to predict chromatin profiles from long DNA sequences and was unable to leverage network graph information.

To strengthen the role of multi-relational and structural information for the network feature learning of miRNAs and genes, we utilize a heterogeneous graph transformer (HGT) to effectively extract complex heterogeneous network information. Finally, we combine a MLP layer and a bilinear function to obtain the MTIs predicting scores. Our experimental results support that MiRGraph conferred significant performance improvements in MTIs predictions over the state-of-the-art methods. Its substructure TransCNN also has a relatively competitive performance when applied alone to distinguish the high functional MTIs without graph structure. Our case studies highlight a candidate oncomir *hsa-miR-181a-5p* in cancer development.

In the future work, we will incorporate more molecular interaction network such as miRNA-gene, miRNA-circRNA and so on, into the representation learning of miRNAs, thereby better understanding the complex functional mechanisms between miRNAs. Also, it is a promising and interesting study to explore the function of miRNAs and its relationship with other molecules in single cell.

Bibliography

[1] David P Bartel. Micrornas: genomics, biogenesis, mechanism, and function. *cell*, 116(2):281–297, 2004.

[2] Sam Griffiths-Jones, Russell J Grocock, Stijn Van Dongen, Alex Bateman, and Anton J Enright. mirbase: microrna sequences, targets and gene nomenclature. *Nucleic acids research*, 34(suppl_1):D140–D144, 2006.

[3] Luca FR Gebert and Ian J MacRae. Regulation of microrna function in animals. *Nature reviews Molecular cell biology*, 20(1):21–37, 2019.

[4] Eric C Lai. Micrornas are complementary to 3 utr sequence motifs that mediate negative post-transcriptional regulation. *Nature genetics*, 30(4):363–364, 2002.

[5] George A Calin and Carlo M Croce. Microrna signatures in human cancers. *Nature reviews cancer*, 6(11):857–866, 2006.

[6] Yong Peng and Carlo M Croce. The role of micrornas in human cancer. *Signal transduction and targeted therapy*, 1(1):1–9, 2016.

[7] Peter Androvic, Lukas Valihrach, Julie Elling, Robert Sjoback, and Mikael Kubista. Two-tailed rt-qpcr: a novel method for highly accurate mirna quantification. *Nucleic acids research*, 45(15):e144–e144, 2017.

[8] Sung Wook Chi, Julie B Zang, Aldo Mele, and Robert B Darnell. Argonaute hits-clip decodes microrna–mrna interaction maps. *Nature*, 460(7254):479–486, 2009.

[9] Markus Hafner, Markus Landthaler, Lukas Burger, Mohsen Khorshid, Jean Hausser, Philipp Berninger, Andrea Rothballer, Manuel Ascano, Anna-Carina Jungkamp, Mathias Munschauer, et al. Transcriptome-wide identification of rna-binding protein and microrna target sites by par-clip. *Cell*, 141(1):129–141, 2010.

[10] Michael Kertesz, Nicola Iovino, Ulrich Unnerstall, Ulrike Gaul, and Eran Segal. The role of site accessibility in microrna target recognition. *Nature genetics*, 39(10):1278–1284, 2007.

[11] Doron Betel, Anjali Koppal, Phaedra Agius, Chris Sander, and Christina Leslie. Comprehensive modeling of microrna targets predicts functional non-conserved and non-canonical sites. *Genome biology*, 11:1–14, 2010.

[12] Anton Enright, Bino John, Ulrike Gaul, Thomas Tuschl, Chris Sander, and Debora Marks. Microrna targets in drosophila. *Genome biology*, 4:1–27, 2003.

[13] Vikram Agarwal, George W Bell, Jin-Wu Nam, and David P Bartel. Predicting effective microrna target sites in mammalian mrnas. *elife*, 4:e05005, 2015.

[14] Byunghan Lee, Junghwan Baek, Seunghyun Park, and Sungroh Yoon. deeptarget: end-to-end learning framework for microrna target prediction using deep recurrent neural networks. In *Proceedings of the 7th ACM international conference on bioinformatics, computational biology, and health informatics*, pages 434–442, 2016.

[15] Albert Pla, Xiangfu Zhong, and Simon Rayner. miraw: A deep learning-based approach to predict microrna targets by analyzing whole microrna transcripts. *PLoS computational biology*, 14(7):e1006185, 2018.

[16] Seonwoo Min, Byunghan Lee, and Sungroh Yoon. Targetnet: functional microrna target prediction with deep neural networks. *Bioinformatics*, 38(3):671–677, 2022.

[17] Sheng-Da Hsu, Feng-Mao Lin, Wei-Yun Wu, Chao Liang, Wei-Chih Huang, Wen-Ling Chan, Wen-Ting Tsai, Goun-Zhou Chen, Chia-Jung Lee, Chih-Min Chiu, et al. mirtarbase: a database curates experimentally validated microrna–target interactions. *Nucleic acids research*, 39(suppl_1):D163–D169, 2011.

[18] Hsi-Yuan Huang, Yang-Chi-Dung Lin, Shidong Cui, Yixian Huang, Yun Tang, Jiatong Xu, Jiayang Bao, Yulin Li, Jia Wen, Huali Zuo, et al. mirtarbase update 2022: an informative resource for experimentally validated mirna–target interactions. *Nucleic acids research*, 50(D1):D222–D230, 2022.

[19] Sean E McGeary, Kathy S Lin, Charlie Y Shi, Thy M Pham, Namita Bisaria, Gina M Kelley, and David P Bartel. The biochemical basis of microrna targeting efficacy. *Science*, 366(6472):eaav1741, 2019.

[20] Jun-Hao Li, Shun Liu, Hui Zhou, Liang-Hu Qu, and Jian-Hua Yang. starbase v2. 0: decoding mirna-cerna, mirna-ncrna and protein–rna interaction networks from large-scale clip-seq data. *Nucleic acids research*, 42(D1):D92–D97, 2014.

[21] Jiawei Luo, Wenjue Ouyang, Cong Shen, and Jie Cai. Multi-relation graph embedding for predicting mirna-target gene interactions by integrating gene sequence information. *IEEE Journal of Biomedical and Health Informatics*, 26(8):4345–4353, 2022.

[22] Weidun Xie, Zetian Zheng, Weitong Zhang, Lei Huang, Qiuzhen Lin, and Ka-Chun Wong. Srg-vote: Predicting mirna-gene relationships via embedding and lstm ensemble. *IEEE Journal of Biomedical and Health Informatics*, 26(8):4335–4344, 2022.

[23] Michael Schlichtkrull, Thomas N Kipf, Peter Bloem, Rianne Van Den Berg, Ivan Titov, and Max Welling. Modeling relational data with graph convolutional networks. In *The Semantic Web: 15th International Conference, ESWC 2018, Heraklion, Crete, Greece, June 3–7, 2018, Proceedings 15*, pages 593–607. Springer, 2018.

[24] Ziniu Hu, Yuxiao Dong, Kuansan Wang, and Yizhou Sun. Heterogeneous graph transformer. In *Proceedings of the web conference 2020*, pages 2704–2710, 2020.

[25] Anjun Ma, Xiaoying Wang, Jingxian Li, Cankun Wang, Tong Xiao, Yuntao Liu, Hao Cheng, Juexin Wang, Yang Li, Yuzhou Chang, et al. Single-cell biological network inference using a heterogeneous graph transformer. *Nature Communications*, 14(1):964, 2023.

[26] Tsung-Yi Lin, Priya Goyal, Ross Girshick, Kaiming He, and Piotr Dollár. Focal loss for dense object detection. In *Proceedings of the IEEE international conference on computer vision*, pages 2980–2988, 2017.

[27] Damian Szklarczyk, Annika L Gable, David Lyon, Alexander Junge, Stefan Wyder, Jaime Huerta-Cepas, Milan Simonovic, Nadezhda T Doncheva, John H Morris, Peer Bork, et al. String v11: protein–protein association networks with increased coverage, supporting functional discovery in genome-wide experimental datasets. *Nucleic acids research*, 47(D1):D607–D613, 2019.

[28] Pei Liu, Jiawei Luo, and Xiangtao Chen. mircom: tensor completion integrating multi-view information to deduce the potential disease-related mirna-mirna pairs. *IEEE/ACM Transactions on Computational Biology and Bioinformatics*, 19(3):1747–1759, 2020.

[29] Qilong Wang, Banggu Wu, Pengfei Zhu, Peihua Li, Wangmeng Zuo, and Qinghua Hu. Eca-net: Efficient channel attention for deep convolutional neural networks. In *Proceedings of the IEEE/CVF conference on computer vision and pattern recognition*, pages 11534–11542, 2020.

[30] Dimitra Karagkouni, Maria D Paraskevopoulou, Serafeim Chatzopoulos, Ioannis S Vlachos, Spyros Tastsoglou, Ilias Kanellos, Dimitris Papadimitriou, Ioannis Kavakiotis, Sofia Maniou, Giorgos Skoufos, et al. Diana-tarbase v8: a decade-long collection of experimentally supported mirna–gene interactions. *Nucleic acids research*, 46(D1):D239–D245, 2018.

[31] Kaiming He, Xiangyu Zhang, Shaoqing Ren, and Jian Sun. Delving deep into rectifiers: Surpassing human-level performance on imagenet classification. In *Proceedings of the IEEE international conference on computer vision*, pages 1026–1034, 2015.

[32] Yanan Duan, Yinghui Dong, Rongguang Dang, Zhihui Hu, Ye Yang, Yueyun Hu, and Jianxin Cheng. Mir-122 inhibits epithelial mesenchymal transition by regulating p4ha1 in ovarian cancer cells. *Cell biology international*, 42(11):1564–1574, 2018.

[33] Aimei Li, Wuqi Song, Jun Qian, Yujun Li, Junming He, Qingmeng Zhang, Wenhui Li, Aixia Zhai, Wenping Kao, Yunlong Hu, et al. Mir-122 modulates type i interferon expression through blocking suppressor of cytokine signaling 1. *The international journal of biochemistry & cell biology*, 45(4):858–865, 2013.

[34] Aleksandra Helwak, Grzegorz Kudla, Tatiana Dudnakova, and David Tollervey. Mapping the human mirna interactome by clash reveals frequent noncanonical binding. *Cell*, 153(3):654–665, 2013.

[35] Ming Lu, Bing Shi, Juan Wang, Qun Cao, and Qinghua Cui. Tam: a method for enrichment and depletion analysis of a microrna category in a list of micrornas. *BMC bioinformatics*, 11(1):1–7, 2010.

[36] Žiga Avsec, Vikram Agarwal, Daniel Visentin, Joseph R Ledsam, Agnieszka Grabska-Barwinska, Kyle R Taylor, Yannis Assael, John Jumper, Pushmeet Kohli, and David R Kelley. Effective gene expression prediction from sequence by integrating long-range interactions. *Nature methods*, 18(10):1196–1203, 2021.